Journal Pre-proof

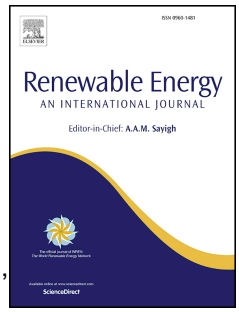

Bioenergy and bioexergy analyses with artificial intelligence application on combustion of recycled hardwood and softwood wastes

Ria Aniza, Wei-Hsin Chen, Christian J.A. Herrera, Rafael Quirino, Mathieu Petrissans, Anelie Petrissans

PII: S0960-1481(24)01953-0

DOI: https://doi.org/10.1016/j.renene.2024.121885

Reference: RENE 121885

To appear in: *Renewable Energy*

Received Date: 6 July 2024

Revised Date: 8 November 2024

Accepted Date: 11 November 2024

Please cite this article as: Aniza R, Chen W-H, Herrera CJA, Quirino R, Petrissans M, Petrissans A, Bioenergy and bioexergy analyses with artificial intelligence application on combustion of recycled hardwood and softwood wastes, *Renewable Energy*, https://doi.org/10.1016/j.renene.2024.121885.

Graphical abstract

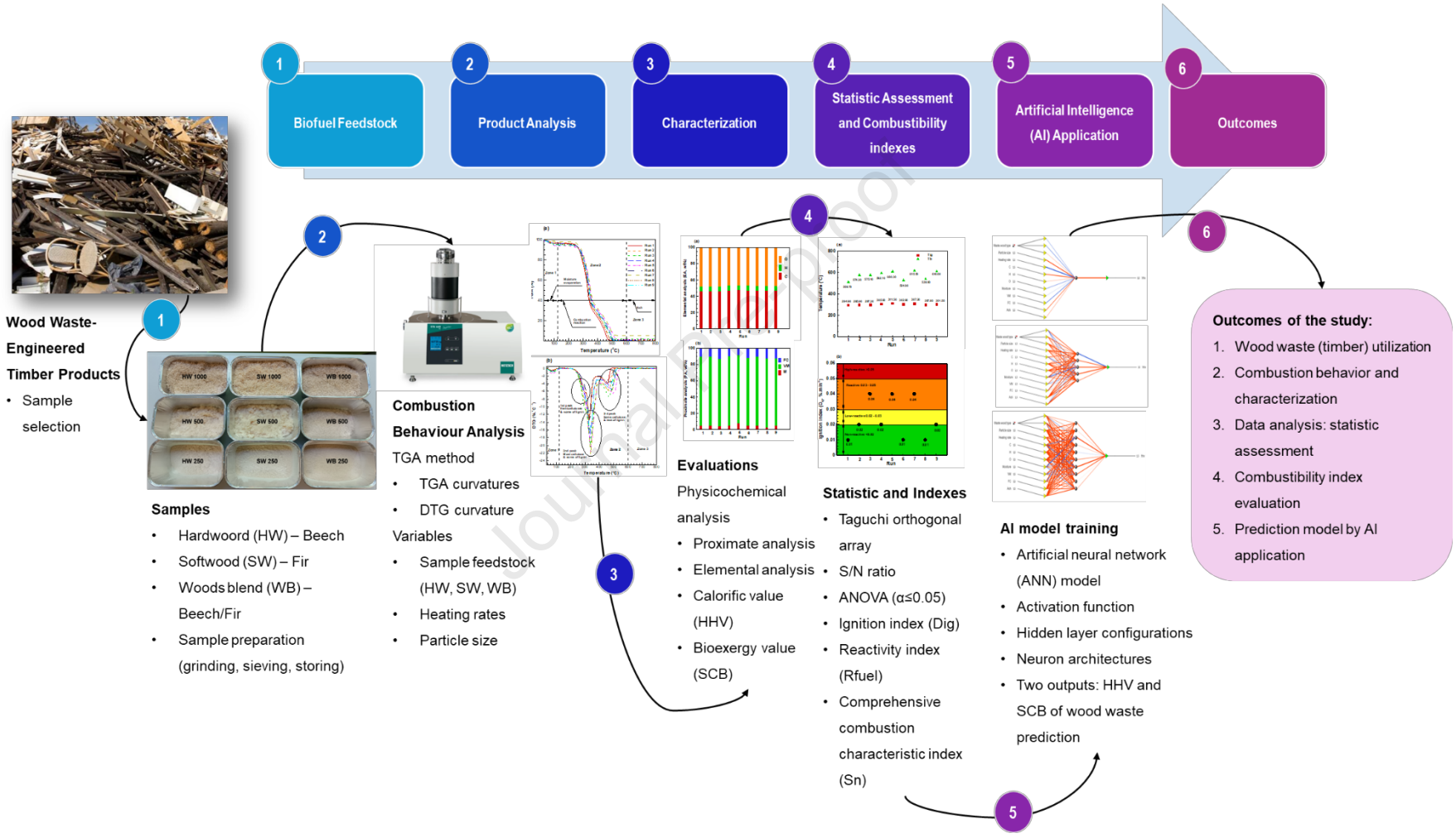

Bioenergy and bioexergy analyses with artificial intelligence application on combustion of recycled hardwood and softwood wastes

Ria Aniza [1,2,3,4], Wei-Hsin Chen [3,5,6,*], Christian J. A. Herrera [7], Rafael Quirino [7], Mathieu Petrissans [1], Anelie Petrissans [1,*]

1. Université de Lorraine, INRAE, LERMAB, F88000, Epinal, France
2. International Doctoral Degree Program in Energy Engineering, National Cheng Kung University, Tainan 701, Taiwan
3. Department of Aeronautics and Astronautics, National Cheng Kung University, Tainan 701, Taiwan
4. Research Center for Energy Conversion and Conservation, National Research and Innovation Agency, Tangerang Selatan 15314, Indonesia
5. Research Center for Smart Sustainable Circular Economy, Tunghai University, Taichung 407, Taiwan
6. Department of Mechanical Engineering, National Chin-Yi University of Technology, Taichung 411, Taiwan
7. Chemistry Department, Georgia Southern University, Statesboro, GA-30460, USA

* Corresponding author; Email: weihsinchen@gmail.com & chenwh@mail.ncku.edu.tw (W.-H.Chen); anelie.petrissans@univ-lorraine.fr (A. Petrissans)

Abstract

Novel biomass bioenergy-bioexergy analyses *via* thermogravimetry analysis and artificial intelligence are employed to evaluate the three biofuels from wood wastes (softwood-SW, hardwood-HW, and woods blend-WB). The chemical characterization of SW has the highest bioenergy (higher heating value – HHV: 18.84 $MJ \cdot kg^{-1}$) and bioexergy (specific chemical bioexergy – SCB: 19.65 $MJ \cdot kg^{-1}$) with the SCB/HHV ratio of wood waste as about 1.043-1.046. The high C-element has a significant influence on the HHV-SCB. The SCB/HHV ratio of wood waste is recognized as about 1.043-1.046. The three distinct zones of wood waste combustion are identified: moisture evaporation (Zone I, up to 110 °C), combustion reaction – degradation of three major lignocellulosic components (hemicelluloses, cellulose, and lignin) at Zone II, 110-600 °C, and ash remains (Zone III, 600-800 °C). The ignition (D_{ig}=0.01-0.04) and fuel reactivity (R_{fuel}=3.82-6.97 $\%\cdot min^{-1}\cdot °C^{-1}$) indexes are evaluated. The comprehensive combustion index ($S_{n:}$>$5\times10^{-7}\%^2\cdot min^{-2}\cdot °C^{-3}$) suggests that wood waste has a better combustion performance than bituminous coal. The statistical evaluation presents that the highest HHV-SCB values are obtained by performing combustion for SW-250 μm at 15 $°C\cdot min^{-1}$. The S/N

ratio and ANOVA results agree that the wood waste type and particle size denote the most influential parameters. The artificial neural network prediction shows an excellent result (R^2=1) with 1 hidden layer and 5 neuron configurations.

Keywords: Wood valorization; biochar; bioenergy-bioexergy; combustibility indexes; Taguchi method; artificial neural network.

Nomenclature

Abbreviations

A	Ash
AI	Artificial intelligence
ANN	Artificial neural network
ANOVA	Analysis of variance
Bioenergy	Biomass energy
Bioexergy	Biomass exergy
Biofuel	Biomass fuel
DoE	Design of experiment
EA	Elemental analysis
EU	European Union
FA	Fiber analysis
FC	Fixed carbon
FSC	Forest Stewardship Council
FTIR	Fourier transform infrared
GC	Gas chromatography
HHV	Higher heating value
HL	Hidden layer
HW	Hardwood
IEA	International Energy Agency
M	Moisture
PA	Proximate analysis
PM	Particulate matter
RE	Relative error

RT	Room temperature
SCB	Specific chemical bioenergy
SW	Softwood
TG	Thermogravimetry (device)
TGA	Thermogravimetry analysis
UN-SDGs	United Nations' Sustainable Development Goals
VM	Volatile matter
WB	Woods blend
WHO	World Health Organization

Symbols

D_{ig}	Ignition index
L_9	Taguchi orthogonal array for nine runs
p	Probability value
R_{fuel}	Fuel reactivity index
S_n	Comprehensive combustion characteristic index
S/N	Signal-to-noise ratio
T_b	Burnout temperature
T_{ig}	Ignition temperature
W	Weight in ANN analysis

Greek letter

α	Confidence level on statistical analysis ($\alpha \leq 0.05$)

1. Introduction

The global emission of CO_2 was reported to reach over 36.8 Gt in 2022, which increased by 0.9% or 321 Mt from the observed point of 2021 [1]. According to the data on CO_2 global emissions in 2022 stated by the International Energy Agency (IEA) [1], this number contributes to the increase of the emissions from coal-based energy sources – increased by 1.6% (from 2021) or 243 Mt, far surpassing the last decade's average growth rate, and achieving a new all-time high level of CO_2 of almost 15.5 Gt. Unfortunately, the increase in fossil fuel usage such as coal is scientifically proven to trigger increases in several issues including environmental (anthropogenic air [2, 3], soil [4], water [5] pollution, global warming [6], extreme weather [7], flood [8], water resource challenges [9], and disruption of land and water ecosystems) [10] and human health (respiratory disorder [11], cancer [12], even premature death [13]).

Wood waste or wood by-products has gained some attention worldwide as a second-generation biomass fuel (biofuel), which may considered a potential sustainable material of lignocellulosic-based biomass for renewable energy production [14, 15]. Generally speaking, the lignocellulosic components define the chemical composition of both hardwood and softwood. The composition of hardwood species is 38-51% cellulose, 17-38% hemicelluloses, 2-31% lignin, and 3% extractives [16, 17]. Softwood species, on the other hand, have a composition of 33-42% cellulose, 22-40% hemicelluloses, 27-32% lignin, and 2-3.5% extractives [18, 19]. One of the thermochemical processes, combustion (**Fig. 1**), is suggested as a viable method for valorizing wood waste into valuable products such as heat. Wood waste direct combustion refers to the conversion process of burning woody waste biomass under a fully oxidative environment such as air or O_2 [20]. Combustion involves several key factors: temperature, heating rate, heating duration, and feedstock composition.

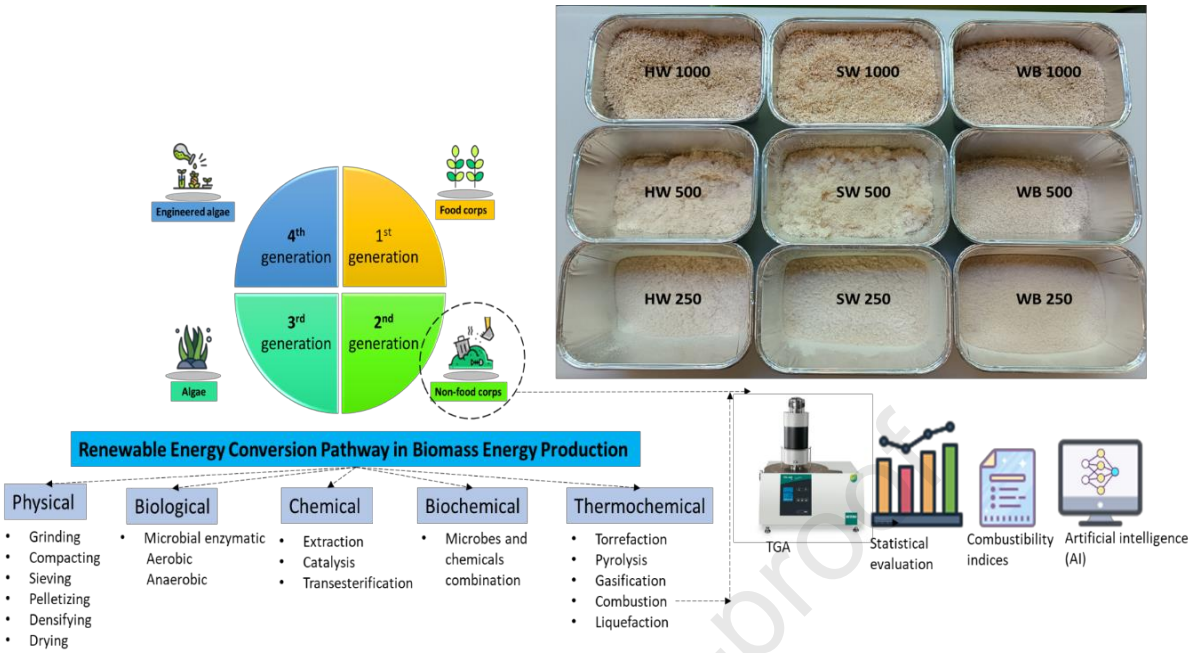

Fig. 1. A recycled wood waste combustion study via TGA was coupled with statistical analysis, combustion indexes, and AI-aided.

If the combustion parameters are not well controlled, it can lead to the generation of particulate matter (PM) or smoke [3] and high CO emissions [2]. Long-term exposure to PM and CO emissions for more than its average level as World Health Organization (WHO) standards 15 μgm^{-3}/24 h, 45 μgm^{-3}/24 h, and 7 μgm^{-3}/24 h for PM 2.5, PM 10, and CO [21], respectively, are reported to be one of the root causes of respiratory disorders (asthma, respiratory inflammation) and even cell death due to DNA damage. Additionally, in some studies, the combustion analysis is crucial for safety reasons and energy conversion systems, such as to prevent fire hazards due to overreactive biofuel on spontaneous ignition [22] and to optimize the combustion process within the reactor [23, 24]. In this matter, evaluating the physicochemical properties, thermodegradation behavior, and combustibility performance by investigating the combustion parameter using integrated TGA and bioenergy-bioexergy analyses to obtain the best condition for bioenergy production ─ avoiding PM or shoot

generation, CO emissions, and considering the safety reasons from wood waste biofuel feedstock is indeed essential.

The TGA method, which uses a thermogravimetry (TG) device, is one of the techniques used to observe the degradation of material as a function of temperature or time [25]. By performing the TGA method, the thermodegradation behavior of biomass feedstock, including combustion, can be fully identified. Some of the valuable information that can be obtained from the TGA method is the degradation curve of mass loss TGA, differential thermogravimetry (DTG), ignition temperature (T_i), and burnout temperature (T_b). Additionally, the biofuel quality during the combustion process can be evaluated by calculating the fuel reactivity (R_{fuel}) and comprehensive combustion index (S_n).

Among the types of bioexergy analysis, SCB is an effective way to evaluate renewable energy in the circular bioeconomy concept from a biomass-based source. SCB focuses on identifying the biofuel's energy according to the chemical composition of the biomass [26]. Previous studies claimed that exergy in biomass can be obtained by calculating the elemental analysis (C, H, O, N, and S elements) and proximate analysis (ash content) [27, 28]. Performing the SCB evaluation, which relies on the second law of thermodynamics on wood valorization ─ can be used to identify the location, amount, quality, and cause of thermodynamic inefficiencies (exergy destructions and losses), which is suggested to fully represent the actual energy within the material compared to higher heating value (HHV) or lower heating value (LHV).

The concept of recycling woody waste into biofuel is considered an effective method that shares the goal of achieving the future United Nations – Sustainable Development Goals (UN-SDGs) affordable and clean energy (SDG7), responsible consumption and production (SDG12), and climate action (SDG13), industry, infrastructure, and innovation (SDG9), as well as align to zero waste principle for managing waste generation. Furthermore, AI accelerates the

148 transition rate to a sustainable energy future by enhancing renewable energy production and
149 development's reliability, affordability, and scalability [29, 30].

150 Numerous studies have been performed on biomass combustion. However, as far as the
151 authors' knowledge, no study has focused intensely on wood waste combustion in terms of
152 bioenergy (HHV) and bioexergy (SCB). There is a lack of knowledge on the related topic of
153 its technology and development. In this matter, a comprehensive study for biofuel production
154 through combustion has not yet been developed while considering the physicochemical,
155 thermodegradation behavior, and combustibility performance. Therefore, this study aims to
156 provide bioenergy and bioexergy analyses of wood waste (**Fig. 1**) *via* TGA in an all-inclusive
157 manner (Taguchi orthogonal array, statistical evaluation, combustibility performance, and AI
158 analysis). This study offers benefits for bridging the current bioenergy technology and
159 advancement gap. Furthermore, it gives researchers with related interests and professionals in
160 the industry a better understanding and helpful information, particularly for the development
161 of renewable bioenergy production and industrial scale-up using bioenergy woody-based
162 materials.

163 ## 2. Materials and methods

164 ### *2.1. Materials*

165 The wood waste of this study was obtained from the timber industries in North-East
166 France. The woods (hardwood: beech - *Fagus sylvatica* and softwood: fir - *Abies alba*) were
167 harvested from the local forest for lumber production. The samples were classified into three
168 types of sample wood waste, including hardwood (HW), softwood (SW), and woods blend
169 (WB, 50-50 wt% mixture of HW and SW, respectively). The commercial high-pressure woody-
170 based briquettes solid biofuel in the European Union (EU) region from raw virgin wood was
171 certified by the Forest Stewardship Council (FSC) to be smokeless, 100% eco-friendly, and

produced without binders-additives with the mixing ratio of 50-50 wt% HW and SW [31]. In this regard, this study attempted to adopt the commercial wood mixing method for the mixture of WB.

2.2. Methods

2.2.1. Sample preparation

The samples were open-air sun-dried for about 24 h. The dried samples were ground and sieved individually to obtain a uniform particle size into three types of sizes, including 250, 500, and 1000 μm [29]. Furthermore, more biomass was broken down by heat transfer at smaller particle sizes of less than 0.5 mm (500 μm), which accelerated the thermochemical process and increased biofuel output [26]. In this manner, the three chosen particle sizes from 250-1000 μm considered appropriate ways to investigate the thermodegradation of biomass. All the samples were stored in sample storage at room temperature (RT) until the analyses were performed.

2.2.2. Design of experiment (DoE)

The Taguchi orthogonal array is a tool for conducting experiments and efficiently optimizing product or process design. The main purpose of Taguchi orthogonal arrays is to create a matrix representing a set of experimental conditions to effectively reduce the number of experimental runs without losing the importance of the variable. Taguchi's methods enable efficient experimentation with minimal trials while providing reliable results. The factors (**Table 1a**) in this research based on the Taguchi method were considered: wood waste type, particle size, and heating rate. Additionally, three levels corresponding to these factors design (1) hardwood (HW), softwood (SW), and woods blend (WB); (2) 250, 500, and 1000 μm; and (3) 10, 15, and 20 $°C \cdot min^{-1}$. The design matrix involving the three factors and three levels of design contained nine runs (L_9) of experiments (**Table 1b**).

196 **Table 1**

197 Design of experiment (DoE) of direct combustion of recycled wood wastes (a) three factors
198 and three levels and (b) Taguchi orthogonal array for nine runs (L_9).

199 **(a)**

Factors	Control parameters	Levels		
		1	2	3
A	Wastes type (%)	Hardwood (100%)	Softwood (100%)	Woods blend [a] (50%:50%)
B	Particle size (µm)	250	500	1000
C	Heating rate (°C·min^{-1})	10	15	20

200 a: woods blend contains 50% hardwood (beech) and 50% softwood (fir)

201 **(b)**

Run	DoE combinations		
	A	B	C
1	Hardwood	250 µm	10 °C·min^{-1}
2	Hardwood	500 µm	15 °C·min^{-1}
3	Hardwood	1000 µm	20 °C·min^{-1}
4	Softwood	250 µm	15 °C·min^{-1}
5	Softwood	500 µm	20 °C·min^{-1}
6	Softwood	1000 µm	10 °C·min^{-1}
7	Woods blend	250 µm	20 °C·min^{-1}
8	Woods blend	500 µm	10 °C·min^{-1}
9	Woods blend	1000 µm	15 °C·min^{-1}

202

203 *2.2.3. Statistical evaluation*

204 The results acquired from the Taguchi orthogonal array were evaluated using the signal-
205 to-noise (*S/N*) ratio and analysis of variance (ANOVA) to identify which parameter and level
206 had significant influences on the bioenergy (HHV) and bioexergy (SCB) values.

207 In terms of the S/N ratio, the HHV and SCB were analyzed for the larger-is-the-better
208 characteristic (Eq. **(1)**) [29], as follows:

$$Sn = -10\log\left({}^{1}/_{y^2}\right) \quad (1)$$

where *y* represents the objective function of HHV or SCB of biofuel.

For ANOVA, the result was observed to calculate the differences between groups. The characteristic of ANOVA was described in Eq. **(2)** [32] as follows:

$$\text{ANOVA: } \alpha \leq 0.05 \quad (2)$$

where α represents a significant level, with 95% confidence and 5% of maximum risk. The lack-of-fit test is used when dealing with data containing replicates or observations with identical x-values. Because discrepancies between the observed response values can only be caused by random variation, replicates are a representation of "pure error". One compares the p-value to the significant level to ascertain whether the model fits the data appropriately. A significance level of 0.05 is typically effective, also known as alpha or α. When a model has an α of 0.05, there is only a 5% chance of finding that the data does not fit the model. In this manner, a 5% significant level was considered to be utilized in this study. Additionally, to quantify the accuracy of the result, the relative error (RE) of data was determined (Eq. **(3)**) [26, 29],

$$RE\ (\%) = \left|\frac{(A-B)}{A}\right| \times 100 \quad (3)$$

where A and B are observed (first trial) and measured (second trial) values, respectively.

2.2.4. Proximate, elemental, and calorific value analyses

Proximate analysis (PA) was performed by applying the ISO 18134-1:2022 [33], ISO 18123:2023 [34], and ISO 18122:2022 [35] for moisture (M), volatile matter (VM), and ash (A) analysis, respectively. Proximate analysis of solid biofuels was using a muffled furnace – Carbolite Furnace CSF 1200. Meanwhile, the fixed carbon (FC) was calculated by difference (Eq. **(4)**) [36].

$$FC\ (\%) = 100\% - M - VM - A \quad (4)$$

Elemental analysis (C, H, O, N, and S) was performed using an automatic elemental analyzer (Thermo Flash Smart Elemental Analyzer). To determine the calorific value, the higher heating values (HHVs) of the sample tests were calculated by employing the HHV in Eq. **(5)** [37], as follows:

$$HHV = 0.3491\,C + 1.1783\,H - 0.1034\,O - 0.0151\,N + 0.1005\,S - 0.0211\,A \quad (5)$$

where C, H, O, N, and S are the chemical compounds in EA and A is the ash content in PA.

2.2.5. Specific chemical bioexergy (SCB)

The bioexergy analysis of this study was evaluated by determining the chemical compound in elemental analysis and considering the ash in proximate analysis. The calculation of the SCB [27, 28] utilized the bioexergy equation in Eq. **(6)**, as follows:

$$SCB = 36.3439\,C + 107.5633\,H - 8.6308\,O + 0.4147\,N + 19.0798\,S - 21.100\,A \quad (6)$$

2.2.6. Combustion experiment via TGA and product analysis via FTIR

The direct combustion of wood waste was carried out using the TG device NETZSCH STA 449 F3 Jupiter. About 5 mg of the sample was loaded into a ceramic crucible about 90 µL size. For instance, the N_2 gas was purged into the system for 100 mL·min^{-1} in 5 min. Then, the sample was heated using three heating rates, including 10, 15, and 20 °C·min^{-1} from RT to 800 °C (**Fig. 1**). The solid remaining in the crucible was considered the ash content. The experiments in this study, including proximate analysis, elemental analysis, calorific value, and direct combustion, were performed in duplicate. The reproducibility of the data was managed at >95% (maximum risk at 5%). Additionally, the Fourier Transform Infrared (FTIR) Spectroscopy FTIR spectra were recorded using FTIR Shimadzu between 4000 and 600 cm^{-1} by the potassium bromide pellet method to analyze the best wood waste type for the combustion process.

2.2.7. Combustion index calculation

(1) Ignition index

The ignition index D_{ig} (%·min^{-3}) was determined as follows [24, 38] (Eq. **(7)**):

$$D_{ig} = \frac{\left(dw/dt\right)_{max}}{(t_{max} \cdot t_{ig})} \quad (7)$$

where $\left(dw/dt\right)_{max}$ (%·min^{-1}) is the maximum combustion rate (DTG curve at the highest peak - DTGmax), t_{max} is the corresponding time when $\left(dw/dt\right)_{max}$ use equation the maximum combustion rate occurs, and t_{ig} was the ignition time. The ignition index implied the potential of accumulated fine fuels to ignite in the presence of a heat source (flammability behavior), demonstrating the fuels' tendency to receive heat and initiate combustion. The low ignition index indicated that the material ignited at high temperatures. In this regard, a higher heat supply was required to ignite the material. In contrast, the high ignition index indicated that the material ignited at low temperatures.

(2) Reactivity index

The combustion reactivity index (R_{fuel}, %·min^{-1}·°C) facilitated the evaluation of the reactivity level of fuel in this study. It may be expressed as follows [39] (Eq. **(8)**):

$$R_{fuel} = \frac{\left(dw/dt\right)_{max}}{T_{max}} \quad (8)$$

where $\left(dw/dt\right)_{max}$ is data in the DTG curve known as DTG*max* (%·min^{-1}). Additionally, T_{max} (°C) corresponded to the peak of the DTG curve. The reactivity index indicates how reactive the fuel could be when the heat source is present. The lowest to highest reactivity index value is about 0.00 to >0.05 %·min^{-1}·°C. There are four distinguished regions in the reactivity index according to the value, including non-reactive (0.00-0.02), low-reactive (0.021-0.03), reactive

(0.031-0.05), and high reactive (>0.051). The highly reactive biofuel is unfavorable because it could trigger incomplete combustion and explosion.

(3) Comprehensive combustion characteristic index

The comprehensive combustion characteristic index (S_n) is a combustion index to evaluate the comprehensive behavior of biofuel combustion [40, 41]. It was defined as (Eq. **(9)**):

$$S_n = \frac{\left(dw/dt\right)_{max}\left(dw/dt\right)_{mean}}{(T_{ig}^2 . T_b)} \quad (9)$$

where $\left(dw/dt\right)_{max}$ and $\left(dw/dt\right)_{mean}$ are the maximum and average weight loss rates, respectively. A higher S_n value indicated a better biofuel combustion performance. Meanwhile, T_{ig} and T_b were the ignition and burnout temperatures, respectively.

2.2.8. Artificial neural network (ANN) analysis

The ANN is one sort of computerized artificial intelligence that mimics how neurons in the human brain process information. ANN provides predictive benefits, such as indirectly detecting complex non-linear connections between variables and taking a small dataset to obtain a high-accuracy result. To validate the ANN model, the trained ANN's predictions of HHV-SCB values were compared to experiment data. Additionally, the sensitivity analysis was automatically calculated during the training process, and the result notified whether the model was overfitting or underfitting. The parameters were designed as input data to determine the influence of the HHV and SCB as the output data. The ten parameters used for feeding the input data include the duplicate of the Taguchi parameters (waste type, particle size, and heating rate-9 runs): 18 data, EA (C-H-O): 18 data (HW, SW, and WB), and PA (M, VM, FC, Ash): 24 data (HW, SW, and WB). The ANN model software used was Megaputer Polyanalyst 6.5. The hidden layer was designed for one layer with 1, 5, and 10 neurons (detailed in supplementary material **Table S1**). The activation functions used in this study were sigmoid and piecewise

linear in the hidden layers and output layer, respectively. The dataset (60 data in total) was divided into 80:20 for training (80%) and testing (20%) [26, 29]. The training algorithm used in this study was quick backpropagation (quick prop) [26]. The three configurations of the ANN model are illustrated in **Fig. 2**.

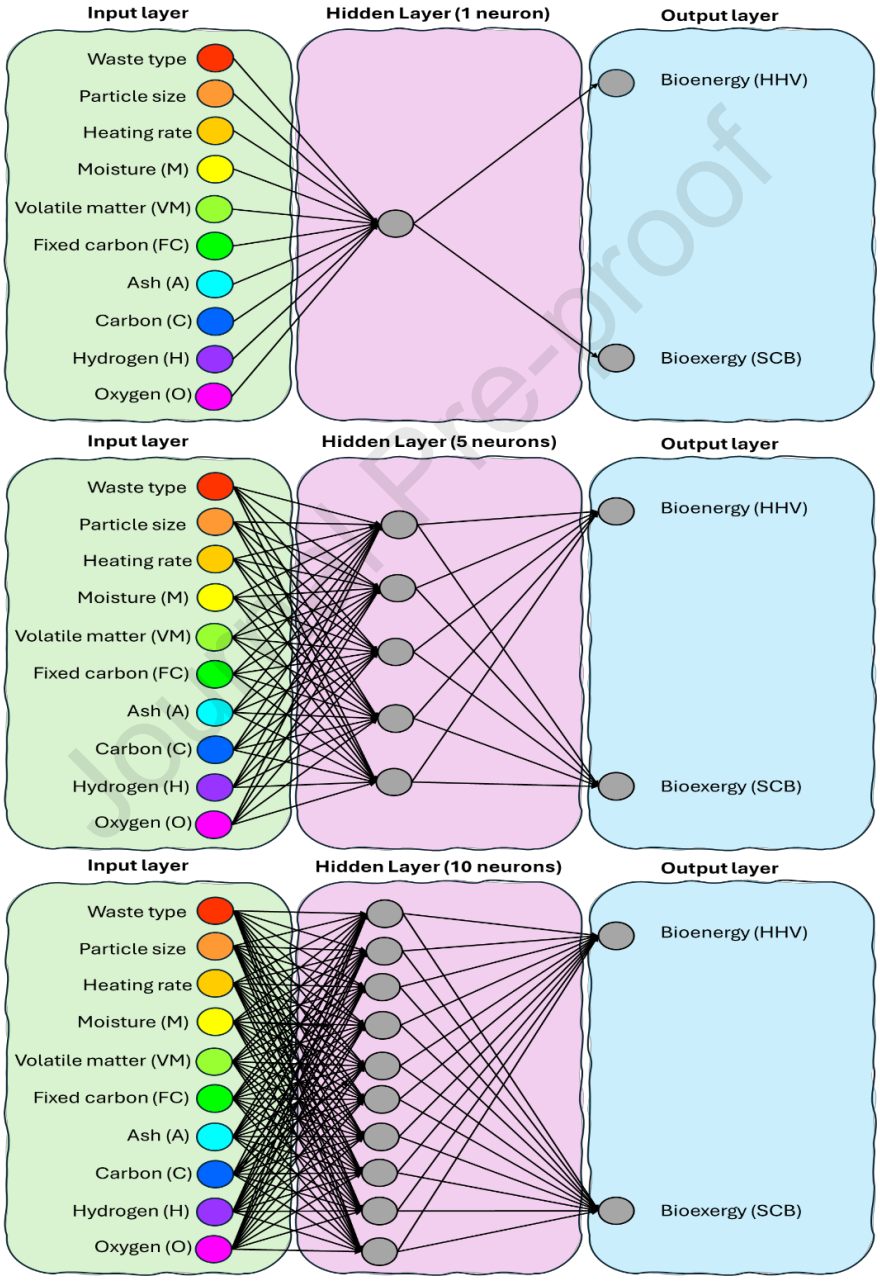

Fig. 2. Configuration of the artificial neural network (ANN) model.

3. Results and discussion

3.1. Properties of wood waste

The initial characterizations of biomass feedstock, including HW, SW, and WB, are described in **Table 2**. For proximate analysis, HW, SW, and WB moisture contents are 5.94, 4.00, and 3.00 wt%, respectively. The low moisture content in biofuel is favorable because it may increase the energy density, thereby improving combustion efficiency. The VM in all samples show > 80wt%, including HW (84.05 wt%), SW (83.50 wt%), and WB (83.67 wt%). A high VM in the sample indicates that the material has a high possibility of solid chemical compounds, such as lignocellulosic components (hemicelluloses, cellulose, and lignin) to devolatilize into gaseous chemical compounds.

Table 2

Raw wood waste properties of proximate analysis, elemental analysis, and bioenergy-bioexergy values.

Biomass properties	**Waste types**		
	Hardwood (HW)	**Softwood (SW)**	**Woods blend (WB)**
Proximate (wt%)			
M	5.94	4.00	3.00
VM	84.05	83.50	83.67
FC	10.00	12.50	13.32
Ash	<0.01	<0.01	0.01
Elemental (wt%)			
C	45.99	47.26	46.58
H	5.77	5.86	5.86
O	45.05	44.36	45.32
N	< 0.05	< 0.05	< 0.05
S	< 0.05	< 0.05	< 0.05
Bioenergy-HHV and bioerxergy-SCB ($MJ \cdot kg^{-1}$)			
HHV	18.20	18.84	18.52

SCB	19.03	19.65	19.32
SCB/HHV ratio	1.046	1.043	1.043

The gaseous compounds from biomass devolatilization can be condensed into liquid biofuel such as bio-oil, biodiesel, bioethanol, etc [26, 42]. In contrast, some studies suggested that the high VM in biomass feedstock tends to have a spontaneous ignition [43] and lower calorific value due to the high O-element. The samples have a slight amount of FC (FC, HW: 10.00 wt%; SW: 12.50 wt%; and WB: 13.32 wt%) but very low ash content (A, HW: <0.01; SW: <0.01; WB: 0.01). The lower FC in biofuel implies that the ash formation is minor. The low ash content in biofuel is favorable because it may prevent clogging in the combustion chamber or utility [44].

Moreover, the EA identification shows that the samples rich in C (HW: 45.99 wt%, SW: 47.26 wt%, WB: 46.58 wt%) and O (HW: 45.05 wt%, SW: 44.36 wt%, WB: 45.32 wt%) elements, but slightly contain H (HW: 5.77 wt%, SW: 5.86 wt%, WB: 5.86 wt%) and very low of N (all samples < 0.05 wt%), and S (all samples < 0.05 wt%) elements. The H/C (0.13 for all samples) and C/O (HW: 0.98, SW: 0.92, and WB: 0.96) ratios indicate that the samples are far from the petroleum characteristics as reported in the Van Krevelen diagram (H/C < 1 and O/C < 0.2) [45]. The raw biomass has the typical atomic values of low H/C and high O/C due to biomass generally containing hemicelluloses, cellulose, and lignin.

3.2. Characterization of wood wastes

3.2.1. Bioenergy and bioexergy analyses

Bioenergy (HHV) and bioexergy (SCB) analyses of wood wastes are identified by analyzing four elements in EA (C, H, O, N, and S) and 1 component of PA (ash). However, the S-element in EA and the ash content in PA in the wood waste of this study reveal that they are negligible (**Table 2**). Accordingly, the terms of S and ash content in **Eq. (6)** for calculating SCB can be ignored. In **Table 2**, the HHV-SCB values of SW (HHV: 18.84 $MJ \cdot kg^{-1}$, SCB: 19.65

337 MJ·kg^{-1}) are identified to possess the highest HHV-SCB values among all samples (WB –
338 HHV: 19.32 MJ·kg^{-1}, SCB: 18.52 MJ·kg^{-1} and HW – HHV: 19.03 MJ·kg^{-1} and SCB: 18.20
339 MJ·kg^{-1}). These phenomena occur due to the SW having a higher C-element within SW (C:
340 47.26 wt%) than WB (C: 46.58 wt%) or HW (C: 45.99 wt%). Although the H-element has the
341 highest coefficient value in the SCB determination (**Eq. (6)**), the amount of H-element in the
342 samples is identified as very low (about <6 wt%). Thus, the H element does not significantly
343 influence the HHV-SCB values of wood waste samples.

344 The FTIR spectrum of the highest HHV-SCB sample of SW is illustrated in **Fig. 3**. The
345 FTIR analysis shows that about three peaks are noticeable at (1st) 1,158.50 cm^{-1}; (2nd) 2,948.63
346 cm^{-1}; and (3rd) 3,425.40 cm^{-1}. According to the FTIR spectrum, the 1st, 2nd, and 3rd peaks occur
347 in the functional group in wavenumber 1,120-1,160 cm^{-1} (fingerprint skeletal region), 2,850-
348 2,950 cm^{-1} (single bond stretch), and 3,350-3,450 cm^{-1} (single bond stretch) correspond to the
349 C-O-C polysaccharide, CH_2 stretching aliphatic group, and OH functional groups, respectively
350 [46]. The 1st peak at 1,158.50 cm^{-1} corresponds to the C-O-C polysaccharide functional group
351 associated with the cellulose chemical compound [47] and the mannose group of
352 hemicelluloses [48, 49]. The mannan-type hemicellulose group (mannose) is a polysaccharide
353 composed of six-carbon sugar glucose. Mannose in softwood can be found as the most
354 abundant sugar compared to other polysaccharide groups [50]. The asymmetric CH_2 stretching
355 vibration is classified as methylene and methine groups in the 2nd peak, correlated to the two
356 types of hemicelluloses (xylan and mannose), cellulose, and lignin [47, 48]. Furthermore, the
357 3rd peak is acknowledged at 3,425.40 cm^{-1}, which is assigned to the OH molecules, associated
358 with cellulose and hemicelluloses [51, 52].

359 Additionally, some absorbance with weak peaks is noticed in between the double and
360 triple bonds region in FTIR spectra corresponding to the alkenes and alkynes, respectively (**Fig.**
361 **3**). The double bond (alkenes) comprises carbon-carbon double bond (-C=C-), which appear in

the moderate band. The stretching vibration of the carbon double bond (-C=C-) is associated with aromatic compounds mostly found in lignin [48, 52]. The alkynes are comprised of carbon-carbon triple bonds (-C≡C-). Few organic compounds exhibit absorption in the triple bond region, where the -C≡C- stretch manifests as a weak band (**Fig. 3**). Organic molecules are considered to have rare triple bonds, but metallic compounds frequently have them. This could be because organic compounds lack valence d-orbitals, making creating triply-bound molecules using metallic atoms challenging. At present, the carbon-carbon triple bond is being massively explored to create organic semiconductors in solar energy systems – photovoltaic applications [53, 54].

Furthermore, the weight of O-element in all samples is identified as a high amount. The high level of O-element in biofuel feedstock is not recommended since it causes some problems, such as instability of combustion reaction [55], and decreased energy density [56]. Thus, the feedstock's deoxygenation prior to biofuel utilization is suggested to avoid rust formation, obtain better combustion performance, and increase the energy density of the feedstock. The biomass sample in the present study shows insignificant amounts of the N- and S-elements and low ash contents. Thus, the influences of N- and S-elements and ash content may be less in HHV-SCB values. In this manner, the terms for S-element and ash content in Eqs. (5) and (6) for HHV-SCB can be ignored. In the HHV calculation (Eq. **(5)**), C-H-S elements are considered energy sources that can be extracted during energy conversion. In contrast, O-N elements have contradictory influences and may not be considered an energy source. The HHV level rises in proportion to the biomass's C-H-S concentrations. In contrast, when the O-N composition of biomass rises, the HHV level falls. Nevertheless, the O-element alone remains the contradictory element for the SCB value, while the N-element has included (C-H-S-N) in the SCB computation (Eq. **(6)**) as an energy source that can be retrieved.

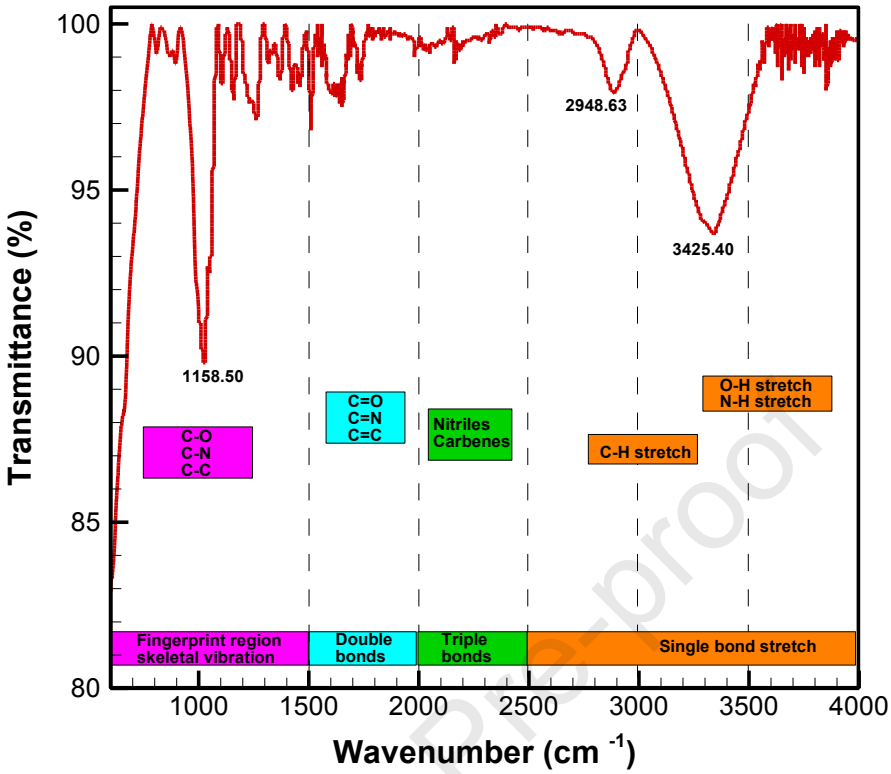

386

387 **Fig. 3.** A record of the FTIR spectrum of SW.

388 According to certain studies, it has been possible to effectively synthesize fuels based on
389 sulfur and nitrogen [57, 58] to meet the world's energy needs. In many applications, the S-N
390 elements are suggested to be energy-storage materials. For instance, S- and N-based fuels may
391 derived from biomass to produce advanced lithium-sulfur (Li-S) batteries [59] and liquid
392 ammonia fuel [60], respectively. Although N and S influences are considered small, in this
393 regard, by considering N-element as an energy source, the SCB computation provides a better
394 insight than HHV to analyze the energy content within the biomass.

395 *3.2.2. Taguchi method analysis*

396 The Taguchi method aims to achieve a favorable product quality by design. The system
397 design can reduce the number of experiments, time, energy, and cost by selecting the desirable
398 factors (variable) and levels (variable intensity). The significant and insignificant parameters

399 that influence the outcomes can be adequately evaluated. By doing so, further investigation of
400 the topic can be accomplished without repeating the same insignificant parameters. This
401 condition can make the concept of further research more novel and explorative.

402 Similar to the biomass feedstock with the bulk size, the feedstock with three different
403 sizes (250, 500, and 1000 μm) has the typical characteristic (detailed in supplementary material
404 **Fig. S1**) that is rich in C (47.32-48.82 wt%) and O (45.18-36.87 wt%), but very low in H (5.55-
405 6.27 wt%) elements. The proximate analysis also suggests that the samples contain very high
406 VM (> 80 wt%), few FC (< 14 wt%), slightly M (< 9 wt%), and negligible A (< 0.01 wt%). In
407 this regard, the combustibility performance of wood waste is dominated by the volatile
408 compounds (VM) within biomass compared to the non-volatile compounds such as FC. To
409 improve the energy density of the solid biofuel, some of the previous studies demonstrated
410 several types of thermochemical conversion, such as torrefaction in low-temperature operation
411 (< 350 °C) [15, 61] and pyrolysis (medium to high-temperature operation, 350-800 °C) [26,
412 29].

413 The HHV determination, according to the Taguchi orthogonal array, is 18.33-19.04
414 $MJ \cdot kg^{-1}$. Meanwhile, SCB is 19.15-19.85 $MJ \cdot kg^{-1}$. These results (SCB: 19.15-19.85 $MJ \cdot kg^{-1}$)
415 are aligned with the exergy of previous studies for alder-fir sawdust (SCB: 20.89 $MJ \cdot kg^{-1}$),
416 beech bark (SCB: 19.63 $MJ \cdot kg^{-1}$), and wood residue (SCB: 20.15 $MJ \cdot kg^{-1}$) [27]. Compared to
417 the biowaste from a previous study using a raw sample of mushroom log waste (12.48 $MJ \cdot kg^{-1}$) [26], this study shows better results of SCB of raw biomass wood waste, about a 35-39 %
419 increase. The correlation between HHV and SCB is noticed due to the similarity of the analysis,
420 depending on the elemental and proximate analyses. The HHV calculation involves elemental
421 components (CHONS) and proximate analysis (ash content) on a dry basis. Likewise, a similar
422 identification occurs in SCB, which involves elemental and proximate components. According
423 to **Fig. 4**, the linear correlation is acknowledged between HHV and SCB. The SCB value

424 increases when the HHV value increases. This phenomenon occurs in all samples of wood
425 waste feedstocks. This linear correlation can be expressed in a ratio of SCB/HHV.

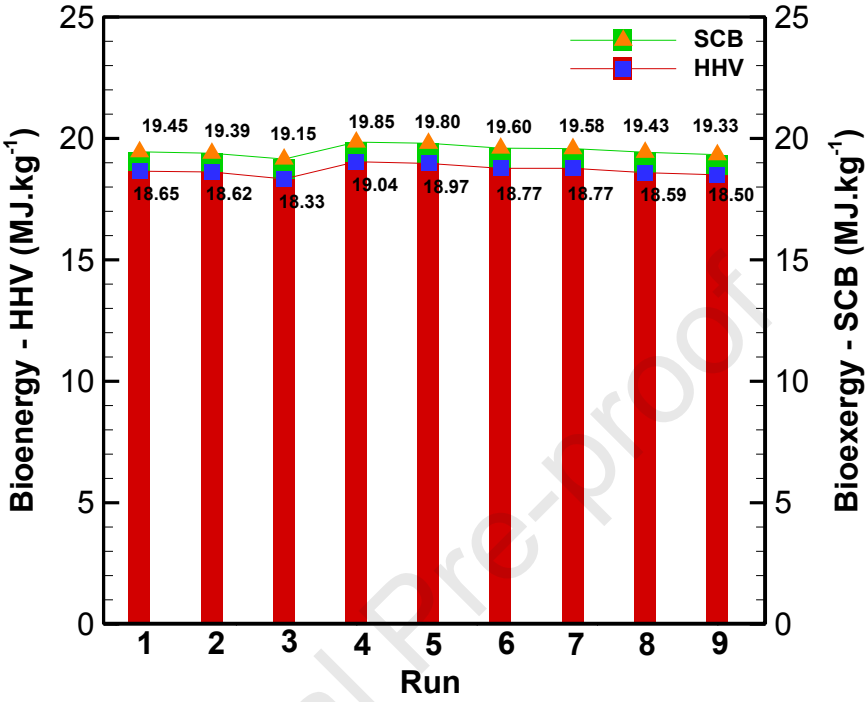

426

427 **Fig. 4.** Bioenergy (HHV) and bioexergy (SCB) values of wood waste according to the Taguchi
428 orthogonal array.

429

430 The SCB/HHV ratio in **Table 2** indicates that the ratio value of HHV and SCB is 1.043-
431 1.046. The highest HHV value (HHV-SW) coincides with the highest SCB value (SCB-SW),
432 and the lowest HHV value (HHV-HW) coincides with the lowest SCB value (SCB-HW) (**Fig.**
433 **4**). The typical evaluation of the energy density using HHV commonly applied for the biofuel
434 product can be corrected by the SCB value through HHV = 1.043-1.046 × SCB. This result is
435 similar to a previous study by Zhang et al. [62] that investigated the connection between exergy
436 and HHV of rice residue. The study revealed that the exergy has a higher value of HHV with a
437 detailed expression of exergy (kJ·kg^{-1}) $Ex = 1312.038 + 0.977\ HHV$.

In the biofuel field, the current indicator used to determine the quality of the material for renewable bioenergy production is the HHV value [15, 37]. However, the SCB analysis, using wood waste as the sample feedstock, reveals that the actual energy within the material is about 1.043-1.046 fold of HHV. The ratio of the SCB/HHV (1.043-1.046) indicates that the number range can be utilized as the factor correction on energy yield calculation. To minimize the error and avoid calculation failure, the result implies that the researcher and industrial practitioner should know vital information about the SCB/HHV ratio to determine the energy balance and production cost using renewable bioenergy feedstock.

3.3. Thermodegradation behavior of wood waste under the combustion process

The behavior of thermodegradation of wood waste under the combustion process is described in three conditions: wood waste, particle size, and heating rate (see the supplementary material **Fig. S2**). The thermodegradation behavior of 9 runs of wood waste (HW, SW, and WB) during the combustion process presents insignificant differences. This may be due to the similarity of the chemical element composition of the three wood wastes. Unlike the inert process of torrefaction or pyrolysis energy conversion, all organic chemical elements, including the three major lignocellulosic components, such as hemicelluloses, cellulose, and lignin, will burn completely during complete combustion to produce CO_2 and H_2O. Therefore, the thermodegradation behavior of the three components shows no apparent difference in TGA/DTG curves. Hemicelluloses and cellulose will thermally degrade in lower temperatures, around 200-315 °C and 300-400 °C, respectively. In contrast, lignin will thermally degrade in a wide temperature range of about 150-600 °C.

The EA in **Table 2** is performed in duplicate, revealing that the N and S elements are very low. The N and S elements are identified at around < 0.05 for all the samples. These phenomena suggest that the wood waste sample has an excellent chemical characteristic as a combustion feedstock. Thus, the chance of producing NOx and SOx from these samples during

463 combustion is relatively low. A few investigations suggest that short-term exposure to NOx and
464 SOx might cause respiratory diseases, such as reduced pulmonary function, increased lung
465 inflammation, and compromised immune system function [63, 64]. In this regard, choosing
466 wood waste as a feedstock is an appropriate step to produce potential environmentally friendly
467 biofuel through combustion conversion. The combustion via TGA of the nine samples exhibits
468 a typical pattern of more than 80 wt% from 110 to 600 °C of VM release during
469 devolatilization. Simultaneously, at temperatures >600 °C, the ash is formed after the FC is
470 burned completely.

471 Degradation zones of the wood waste are distinguishably identified in **Fig. 5**. The three
472 zones can be noticed from TGA curves in **Fig. 5a**. Zone 1 occurs at about RT to 110 °C, where
473 the moisture content evaporates. Zone 2 occurs at about 110-600 °C, where the activity of the
474 combustion reaction is significantly detected. In Zone 2, two to three peaks are recognized from
475 DTG curves (**Fig. 5b**), where the first peak appears between 250-300 °C (Runs 1, 6, and 8,
476 with the lowest heating rate at 10 °C·min^{-1}) which corresponds to the thermodegradation of
477 lignocellulosic chemical compounds with light molecular weight (hemicelluloses) and some
478 lignin. The second peak appears at about 300-400 °C (Runs 3, 5, and 7 with the highest heating
479 rate at 20 °C·min^{-1}) which corresponds to the thermodegradation of mostly cellulose and some
480 lignin. The third peak appears at about 400-550 °C for all the Runs which corresponds to the
481 thermodegradation of slightly cellulose and the rest of the lignin. The DTG curve reveals that
482 the higher heating influences the significant mass loss rate [15, 65].

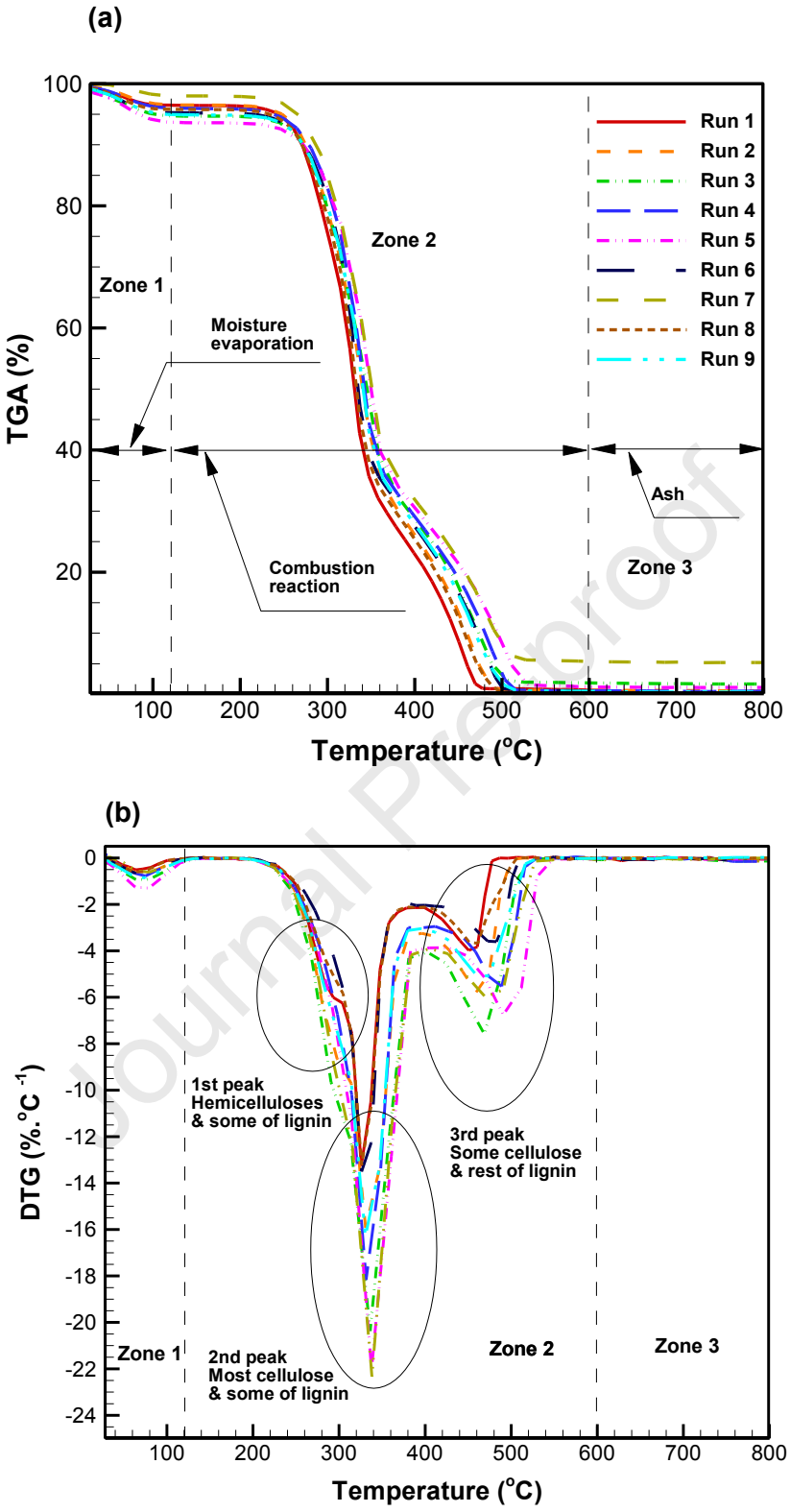

483

484 **Fig. 5.** Combustion zone of (a) TGA and (b) DTG curvatures of wood waste *via* TGA approach.

485

Additionally, Zone 3 (600-800 °C) reveals no degradation (TGA) or peak (DTG) detected. This circumstance suggests that the FC has entirely burned and that ash is the only solid matter left (ash remains). The TGA curves show that Runs 3, 5, and 7, with the highest heating rate, have higher ash contents among the runs. It may be due to the combustion process having less time to burn the entire biomass. Therefore, the solid remains are detected higher than those with lower heating rates. Moreover, the Runs with the lower heating rate (Runs 1, 6, and 8) illustrate that the peaks obtained are one extra in an early stage of the combustion process among other Runs. These conditions imply that the combustible component in the early stage can be evaluated using a lower heating. The ash formation of Runs 1, 6, and 8 also shows an insignificant amount – implying that the complete combustion is more pronounced. Unfortunately, the drawback of using the lower heating may lead to a more time-consuming process, equal to the energy consumption for the electricity supply to the TGA equipment and experimental cost.

3.4. Combustibility of wood waste in terms of combustion indices

The combustibility of biomass fuel refers to its ability to undergo combustion, releasing heat energy in the process. The chemical composition of biomass, particularly the presence of volatile organic compounds, influences its combustibility. As seen in **Fig. 6**, the ignition index (D_{ig}) value increases as the heating rate for the combustion process increases [66]. The ignition index (D_{ig}) measures a material's susceptibility to ignition under specific conditions. When the heating rate is increased, it means that the material is being heated at a faster rate. This can lead to several changes in the ignition process, including reducing heat transfer duration, reducing volatile matter release, and accelerating the chemical reaction. This is the primary reason why the ignition index increases accordingly.

A high ignition index at the same heating rate supply suggests that the material is more likely to ignite at lower temperatures. This phenomenon implies that the material requires less

energy or heat than materials with lower ignition indexes to initiate the ignition process. Additionally, the criterion of self-ignition is classified into four classes, including non-reactive (D_{ig} 0.00-0.02), low-reactive (D_{ig} 0.021-0.03), reactive (D_{ig} 0.031-0.05), and high-reactive (>0.051).

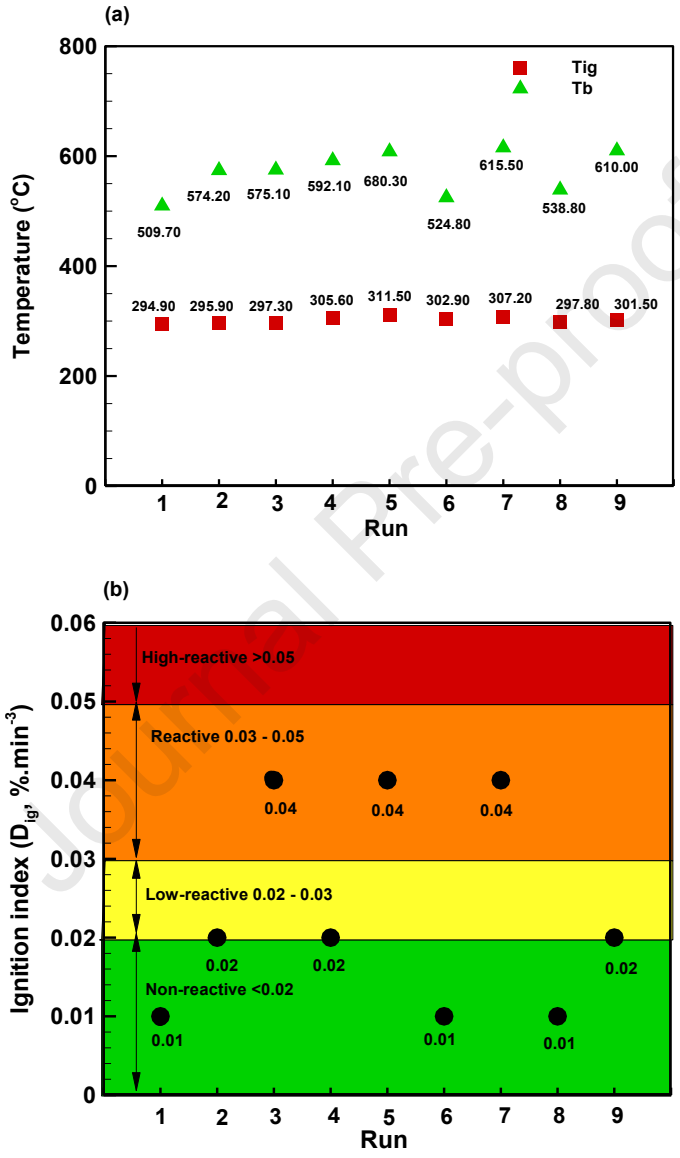

Fig. 6. Ignition and burnout temperature (a) and Ignition index (D_{ig}) (b) of wood waste.

Among the Runs in the Taguchi method, Run 1 (HW 250), 6 (SW 1000), and 8 (WB 500) utilize the lowest heating rate (HR) of 10 °C·min^{-1} have D_{ig} values of 0.01 which belongs to the non-reactive region; Run 2 (HW 500), 4 (SW 250), and 9 (WB 1000) utilize the medium

heating rate (HR) of 15 °C·min^{-1} precisely have D_{ig} of 0.02 which indicates in the low reactive region, and run 3 (HW 1000), 5 (SW 500), and 7 (WB 250) utilize the highest heating rate (HR) of 20 °C·min^{-1} have D_{ig} values of 0.04 which suggests belonging to the reactive region. This implies that the higher heating rate of the combustion process may provide a higher ignition index of the material, which proves the ignition index theory [39]. According to the study, the higher heating rate (>20 °C·min^{-1}) is not recommended since it may initiate the reactivity index value to reach out of the high-reactivity region. Additionally, due to the high volatile content of biomass, it is particularly vulnerable to devolatilization and subsequent volatile combustion in the surrounding gas, which makes these sub-mechanisms much more predominant in the behavior of biomass ignition and combustion. Thus, the highly reactive biofuel (>0.051) is not suggested due to safety concerns (fire, explosion), handling challenges (transporting, storing, packaging), and environmental impacts (air pollution).

The reactivity fuel index analysis illustrates that the higher the heating rate, the higher the reactivity fuel index (R_{fuel}) (detailed in supplementary material **Fig. S3**). The R_{fuel} index values of the wood waste are about 3.82-6.97 %·min^{-1}·°C^{-1}. This result implies that the lowest heating rate (10 °C·min^{-1}) may utilize about 3.82 wt% per minute of biofuel. In contrast, the highest heating rate (20 °C·min^{-1}) may utilize about 6.97 wt% per minute of biofuel. The comprehensive combustion index (S_n) or combustibility index values of wood waste are about 3.20–9.37 × 10^{-7} %^{2}·min^{-2}·°C^{-3}. The results in the present study for S_n index are higher than the results from a previous study of biomass/bituminous coal (<5 × 10^{-7} %^{2}·min^{-2}·°C^{-3}) by Liu et al. [55]. The higher S_n value of wood waste for biofuel production demonstrates that biomass has better combustion performance than solid fossil fuels such as coal.

3.5. Statistical evaluation (bioenergy and bioexergy)

The criterion (larger-is-the-better characteristic of the *S/N* ratio) explains that the larger the value for the corresponding outcome in the matrix of Taguchi, the more favorable the research results are. Additionally, the criterion in ANOVA analysis is fixed with the significant value (α) ≥ 0.05, by means the parameter is considered to be significant when the P-value $\leq \alpha$ ($P \leq 0.05$; 5% risk). In the analysis of the *S/N* ratio for HHV, the results show that the wood waste type has the highest influence (delta) (see supplementary material **Table S2**) by 0.18, followed by particle size 0.13, then the heating rate 0.02 (insignificant). Align with the S/N ratio, the ANOVA analysis also shows that wood waste type has a higher influence (*F*: 29.93), with a significant value (*P*) of about 0.032, followed by particle size (*P*: 0.061) and heating rate (0.727). Likewise, in the *S/N* ratio for SCB (see supplementary material **Table S2**), the result describes that wood waste type (delta: 0.19) has a higher value of influence, followed by particle size (delta: 0.12) and heating rate (delta: 0.01). Moreover, the ANOVA analysis for SCB shows that wood waste type and particle size significantly influence about 53.53 and 20.67, with *p*-values of 0.018 and 0.046, respectively. Meanwhile, the heating rate is recognized as an insignificant parameter. For the optimum result, the highest HHV and SCB are obtained by experimenting with waste type level 2 (softwood), particle size level 1 (250 μm), and heating rate (insignificant) level 2 (15 °C·min^{-1}). The optimum results are combined in Run 4 of the Taguchi orthogonal array.

3.6. ANN analysis for bioenergy and bioexergy prediction

The AI-ANN analysis is carried out with the configuration of one hidden layer (HL) but in three different configurations, including 1, 5, and 10 neurons (N) (detailed in supplementary material **Table S3**). The number of neurons is considered by the number of input parameters [61, 67]. Although the ANN analysis has no fixed rules to train the model, the convenient way to decide the neuron in the hidden layer is by determining the number of

neurons based on the amount of the input layer. The five input parameters, including wood waste type, particle size, heating rate, elemental analysis (C, H, O), and proximate analysis (M, VM, FC, and A), are simulated to predict the output result. Therefore, the neurons to accommodate the input data are considered about 1 (5×0=1), 5 (5×1=5), and (5×2=10).

The training specification of the models shows that the three configurations for HHV prediction have excellent results with a fit-quality value (R^2) of precisely 1.0000. The standard deviation values for the three configurations for HHV model prediction are 0.000080, 0.000013, and 0.000022 for 1HL-1N, 1HL-5N, and 1HL-10N, respectively. The model with 1HL-1N configuration shows that the heating rate is the most significant parameter that influences the HHV prediction. However, the other two prediction models (1HL-5N and 1HL-10N) show that waste type is the most prominent input parameter. Meanwhile, the standard deviation for the SCB model prediction (R^2=1.0000) with the configuration of 1HL-1N, 1HL-5N, and 1HL-10N are 0.014582, 0.000014, and 0.000015, respectively. The three configurations agree that the waste type is the most influential parameter for SCB prediction.

Among the configurations, the best result of the ANN model for HHV and SCB model predictions with the lowest standard deviation is obtained using a 1 HL with 5 N for HHV with the fit quality precisely (R^2) 1. In this regard, the wood waste type is the most influence factor in bioenergy analysis (HHV), followed by FC, O, C, H, particle size, A, heating rate, VM, and M. Likewise, the configuration of 1HL with 5N illustrates the best result prediction for the bioexergy analysis (SCB). The most influential parameters are wood waste type, followed by H, FC, C, O, A, particle size, heating rate, M, and VM. The validation of the model shows that all the models are not underfitting or overfitting. The values between the experiment data and the ANN model (**Table 3**) reveal that the configuration using the formula of 1HL and 5N is suitable for executing the wood waste combustion in this study. In this manner, the models are considered to be well-trained. Compared to the previous studies in the bioenergy production

field (detailed in supplementary material **Table S4**), the present study shows the best results. Some previous studies showed that fewer hidden layers and neurons would provide the best-fit quality of the model [26, 68]. However, in the present study, the number of input parameters is about five in general, but in the overall calculation, the input parameters are 10 in total. For 1HL with 1N, excellent results are obtained with R^2=1. Nevertheless, the stopping criterion describes the maximum epoch that is reached. This result implies that the model reaches the saturation process. Additionally, the higher epoch in the training model in machine learning may lead the model to the underfit or overfit level [29]. Moreover, the 1HL with 10 N displays good results, but the standard deviations for HHV and SCB prediction models are higher than 1HL with 5N. These results indicate that providing more neurons in the hidden layer does not necessarily improve the model prediction. Likewise, the fewer neurons in a hidden layer may lead to the model having a higher standard deviation level due to insufficient neurons to execute the task. This phenomenon implies that 1 neuron is insufficient in this study, but 10 neurons are abundant to accommodate the model prediction. The optimum for five neurons to execute the task is considered ideal in the ANN model prediction of this study.

611 **Table 3**

612 ANN training numerical analysis using 1HL-5N configuration compared to the experiment data.

Wood waste	Particle size	Heating rate	C	H	O	HHV	SCB	M	VM	FC	A	*ANN (HHV)	*ANN (SCB)
Hardwood	250	10	46.130	6.030	44.100	18.649	19.445	4.950	84.219	10.831	0.000	18.649	19.445
Hardwood	500	15	45.880	5.850	41.440	18.625	19.390	4.950	84.219	10.831	0.000	18.625	19.390
Hardwood	1000	20	45.880	5.900	44.880	18.328	19.147	4.000	82.292	13.708	0.000	18.328	19.147
Softwood	250	15	47.020	6.180	45.080	19.035	19.846	5.000	85.263	9.737	0.000	19.035	19.846
Softwood	500	20	47.380	5.950	44.270	18.974	19.799	8.000	83.696	8.284	0.020	18.974	19.799
Softwood	1000	10	47.190	5.820	44.100	18.772	19.605	4.950	83.167	11.883	0.000	18.772	19.605
Wood blends	250	20	46.500	6.110	45.080	18.771	19.581	5.000	84.211	10.789	0.000	18.771	19.581
Wood blends	500	10	46.650	5.980	45.810	18.595	19.433	2.970	84.541	12.479	0.010	18.595	19.433
Wood blends	1000	15	46.630	5.770	44.300	18.497	19.330	4.950	82.292	12.748	0.010	18.497	19.330

613 Particle size (μm)
614 Heating rate ($°C \cdot min^{-1}$)
615 HHV and SCB ($MJ \cdot kg^{-1}$)
616 Standard deviation (SD): HHV (0.000013) and SCB (0.000014)
617 *: ANN model prediction

4. Conclusions

This study has explored wood wastes (HW, SW, and WB) for the behavior of combustion thermodegradation via the TGA method integrated with the Taguchi orthogonal, statistical analysis, combustibility indexes, and AI model prediction. The physicochemical analyses show that all wood waste feedstock is high in VM (>80 wt%), rich in C and O, but low in ash, N, and S contents. The evaluation shows that the SCB is typically higher (about > 19 $MJ \cdot kg^{-1}$) than HHV (about 18 $MJ \cdot kg^{-1}$), with SW reported to possess the highest HHV (18.84 $MJ \cdot kg^{-1}$) and SCB (19.65 $MJ \cdot kg^{-1}$) values. The TGA/DTG curves obtained, using typical heating rates of 10, 15, and 20 $°C \cdot min^{-1}$, suggest there are 3 zones distinguished, and hemicelluloses (< 275 °C), while cellulose and lignin degradation have more way to undergo in about 275–600 °C. The combustibility indexes indicate that wood waste has 4 classes of ignition index (non-reactive to high-reactive), reactivity fuel index at higher heating rate utilizing more feedstock (3.82–6.97 $\%\cdot min^{-1}\cdot °C^{-1}$), comprehensive combustion characteristic index of wood waste has better combustion performance than solid fossil fuel of bituminous coal. Unlike the heating rate, the wood waste type and particle size significantly influence the HHV and SCB. The optimum Run is achieved with SW250 at 20 $°C \cdot min^{-1}$ heating rate. The ANN model with 1HL–5N configuration successfully predicts the values of HHV and SCB with excellent fit-quality values (R^2=1). This study has limitations on the molecular interaction of lignocellulosic components during the combustion conversion process. However, because the exploration is not feasible to Run by TGA only, this study's findings offer new potential information for further investigation. Research on kinetics, by-products in molecular approaches, and catalytic co-combustion are potential topics for future work.

Acknowledgments

The authors gratefully acknowledge the financial support under the program ANR-11-LABEX-0002-01 (Lab of Excellence ARBRE) in France, and the FACE Foundation, iCemiture (NSF-IRES 1952402), and Georgia Southern University. The authors also acknowledge the financial support of the National Science and Technology Council, Taiwan, R.O.C., under the contracts NSTC 113-2218-E-006-012- and NSTC 113-2218-E-002-029- for this research. This research is also supported in part by Higher Education Sprout Project, Ministry of Education to the Headquarters of University Advancement at National Cheng Kung University (NCKU).

References

[1] IEA, CO2 Emission in 2022, Growth in emissions lower than feared, International Energy Agency (IAE) 2022.
[2] Y.-Y. Lee, S.-L. Lin, R. Aniza, C.-S. Yuan, Reduction of Atmospheric PM2.5 Level by Restricting the Idling Operation of Buses in a Busy Station, Aerosol and Air Quality Research 17(10) (2017) 2424-2437.
[3] S.-L. Lin, R. Aniza, Y.-Y. Lee, C.-L. Wang, Reduction of traditional pollutants and polychlorinated dibenzo-p-dioxins and dibenzofurans emitted from a diesel engine generator equipped with a catalytic ceramic fiber filter system, Clean Technologies and Environmental Policy 20(6) (2018) 1297-1309.
[4] X. Nie, T. Zhao, Y. Su, Fossil fuel carbon contamination impacts soil organic carbon estimation in cropland, CATENA 196 (2021) 104889.
[5] Y. Su, Y. Liang, L. Chai, Z. Han, S. Ma, J. Lyu, Z. Li, L. Yang, Water Degradation by China's Fossil Fuels Production: A Life Cycle Assessment Based on an Input–Output Model, Sustainability, 2019.
[6] A. Boretti, Continued fossil fuel emissions and cognition impairment, International Journal of Global Warming 24(1) (2021) 86-90.
[7] P. Dai, J. Nie, Robust Expansion of Extreme Midlatitude Storms Under Global Warming, Geophysical Research Letters 49(10) (2022) e2022GL099007.
[8] H. Cho, Climate Change Risk Assessment for Kurunegala, Sri Lanka: Water and Heat Waves, Climate, 2020.
[9] E. Dubois, M. Larocque, S. Gagné, M. Braun, Climate Change Impacts on Groundwater Recharge in Cold and Humid Climates: Controlling Processes and Thresholds, Climate, 2022.
[10] X. Ma, T. Zhang, C. Ji, Y. Zhai, X. Shen, J. Hong, Threats to human health and ecosystem: Looking for air-pollution related damage since 1990, Renewable and Sustainable Energy Reviews 145 (2021) 111146.
[11] P.J. Landrigan, S. Fisher, M.E. Kenny, B. Gedeon, L. Bryan, J. Mu, D. Bellinger, A replicable strategy for mapping air pollution's community-level health impacts and catalyzing prevention, Environmental Health 21(1) (2022) 70.
[12] C. Rublee, J. Bikomeye, S. Rao, M. Husain, K. Beyer, Climate mitigation and adaptation is cancer prevention and control, The Journal of Climate Change and Health 10 (2023) 100209.

[13] K. Vohra, A. Vodonos, J. Schwartz, E.A. Marais, M.P. Sulprizio, L.J. Mickley, Global mortality from outdoor fine particle pollution generated by fossil fuel combustion: Results from GEOS-Chem, Environmental Research 195 (2021) 110754.
[14] Y.-Y. Lin, W.-H. Chen, B. Colin, A. Petrissans, R. Quirino, M. Pétrissans, Thermodegradation characterization of hardwoods and softwoods in torrefaction and transition zone between torrefaction and pyrolysis, Fuel 310 (2022) 122281.
[15] A. Petrissans, Y.-Y. Lin, T. Nguyen, B. Colin, R. Quirino, P. Rios-Teixeira, W.-H. Chen, M. Pétrissans, Influence of the heating rate on the thermodegradation during the mild pyrolysis of the wood, Wood Material Science & Engineering 18 (2022) 1-10.
[16] J. Hamada, A. Pétrissans, F. Mothe, P. Gérardin, M. Pétrissans, European oak's growth rings properties: density distribution and thermal behavior analysis of early- and latewood, Innovation in woodworking industry and engineering design 2 (2015) 11-17.
[17] W. Schutyser, T. Renders, G. Van den Bossche, S. Van den Bosch, S.-F. Koelewijn, T. Ennaert, B.F. Sels, Catalysis in Lignocellulosic Biorefineries: The Case of Lignin Conversion, Nanotechnology in Catalysis2017, pp. 537-584.
[18] A. Petrissans, R. Younsi, M. Chaouch, P. Gerardin, M. Petrissans, Wood thermodegradation: experimental analysis and modeling of mass loss kinetics, MADERAS: Ciencia y Tecnología 16(2) (2014) 133-148.
[19] M.J. Suota, T.A. da Silva, S.F. Zawadzki, G.L. Sassaki, F.A. Hansel, M. Paleologou, L.P. Ramos, Chemical and structural characterization of hardwood and softwood LignoForce™ lignins, Industrial Crops and Products 173 (2021) 114138.
[20] H. Dai, H. Dai, Green hydrogen production based on the co-combustion of wood biomass and porous media, Applied Energy 324 (2022) 119779.
[21] WHO, WHO air quality guidelines Particulate matter (PM2.5 and PM10), ozone, nitrogen dioxide, sulfur dioxide, and carbon monoxide, World Health Organization Geneva, 2021.
[22] Y. Rahib, V. Leroy-Cancellieri, D. Cancellieri, J. Fayad, J.-L. Rossi, E. Leoni, Study on the combustion indices of forest species using thermogravimetric analysis, Journal of Thermal Analysis and Calorimetry 148(22) (2023) 12919-12935.
[23] A.J. Martyr, D.R. Rogers, Chapter 16 - The combustion process and combustion analysis, in: A.J. Martyr, D.R. Rogers (Eds.), Engine Testing (Fifth Edition), Butterworth-Heinemann, Oxford, 2021, pp. 537-597.
[24] J. Liu, F. Zhong, W. Niu, J. Su, Z. Gao, K. Zhang, Effects of heating rate and gas atmosphere on the pyrolysis and combustion characteristics of different crop residues and the kinetics analysis, Energy 175 (2019) 320-332.
[25] R. Aniza, W.-H. Chen, Y.-Y. Lin, K.-Q. Tran, J.-S. Chang, S.S. Lam, Y.-K. Park, E.E. Kwon, M. Tabatabaei, Independent parallel pyrolysis kinetics of extracted proteins and lipids as well as model carbohydrates in microalgae, Applied Energy 300 (2021) 117372.
[26] W.-H. Chen, R. Aniza, Specific chemical bioexergy and microwave-assisted torrefaction optimization via statistical and artificial intelligence approaches, Fuel 333 (2023) 126524.
[27] G. Song, L. Shen, J. Xiao, Estimating Specific Chemical Exergy of Biomass from Basic Analysis Data, Industrial & Engineering Chemistry Research 50(16) (2011) 9758-9766.
[28] G. Song, L. Shen, J. Xiao, L. Chen, Estimation of Specific Enthalpy and Exergy of Biomass and Coal Ash, Energy Sources, Part A: Recovery, Utilization, and Environmental Effects 35(9) (2013) 809-816.
[29] R. Aniza, W.-H. Chen, F.-C. Yang, A. Pugazhendh, Y. Singh, Integrating Taguchi method and artificial neural network for predicting and maximizing biofuel production via torrefaction and pyrolysis, Bioresource Technology 343 (2022) 126140.
[30] M. Ghaslani, R. Rezaee, O. Aboubakri, E. Sarlaki, T. Hoffmann, A. Maleki, N. Marzban, Lime-assisted hydrothermal humification and carbonization of sugar beet pulp: Unveiling the yield, quality, and phytotoxicity of products, Biofuel Research Journal 11(1) (2024) 2025-2039.

[31] L. HSFuels, RUF EKO briquettes (Harwood softwood mix 50/50) 2018. https://www.hsfuels.co.uk/p39-ruf-eko-briquettes-harwood-softwood-mix-5050. 2024).
[32] T.H. Rizk, Chapter 31 - Analysis of variance, in: A.E.M. Eltorai, T. Liu, R. Chand, S.P. Kalva (Eds.), Translational Interventional Radiology, Academic Press2023, pp. 149-152.
[33] ISO, Solid biofuels - determination of moisture content ISO 18134 - 1: 2022, ISO org, Switzerland 2022.
[34] ISO, Solid biofuels - determination of volatile matter, ISO 18123: 2023, ISO org, Switzerland, 2023.
[35] ISO, Solid biofuels - determination of ash content ISO 18122: 20222, ISO org, Switzerland, 2022.
[36] R. Aniza, W.-H. Chen, E.E. Kwon, Q.-V. Bach, A.T. Hoang, Lignocellulosic biofuel properties and reactivity analyzed by thermogravimetric analysis (TGA) toward zero carbon scheme: A critical review, Energy Conversion and Management: X 22 (2024) 100538.
[37] S.A. Channiwala, P.P. Parikh, A unified correlation for estimating HHV of solid, liquid and gaseous fuels, Fuel 81(8) (2002) 1051-1063.
[38] D. López-González, M.M. Parascanu, M. Fernandez-Lopez, M. Puig-Gamero, G. Soreanu, A. Avalos-Ramírez, J.L. Valverde, L. Sanchez-Silva, Effect of different concentrations of O 2 under inert and CO 2 atmospheres on the swine manure combustion process, Fuel 195 (2017) 23-32.
[39] W. Gao, M. Zhang, H. Wu, Ignition temperatures of various bio-oil based fuel blends and slurry fuels, Fuel 207 (2017) 240-243.
[40] S.Y. Luo, B. Xiao, Z.Q. Hu, S.M. Liu, Y.W. Guan, Experimental study on oxygen-enriched combustion of biomass micro fuel, Energy 34(11) (2009) 1880-1884.
[41] C. Wang, F. Wang, Q. Yang, R. Liang, Thermogravimetric studies of the behavior of wheat straw with added coal during combustion, Biomass and Bioenergy 33(1) (2009) 50-56.
[42] A. Tesfaw, D. Kosebent, E.T. Oner, F. Assefa, Bioethanol production from grass pea and wild oat hydrolysates using S. cerevisiae ETP53, K. marxianus ETP87, and P. fermentans ETP22, Discover Energy 1(1) (2021) 4.
[43] A.T. Conag, J.E.R. Villahermosa, L.K. Cabatingan, A.W. Go, Energy densification of sugarcane leaves through torrefaction under minimized oxidative atmosphere, Energy for Sustainable Development 42 (2018) 160-169.
[44] R. Aniza, W.-H. Chen, A. Pétrissans, A.T. Hoang, V. Ashokkumar, M. Pétrissans, A review of biowaste remediation and valorization for environmental sustainability: Artificial intelligence approach, Environmental Pollution 324 (2023) 121363.
[45] W. Kew, J.W. Blackburn, D.J. Clarke, D. Uhrin, Interactive van Krevelen diagrams - Advanced visualisation of mass spectrometry data of complex mixtures, Rapid Commun Mass Spectrom 31(7) (2017) 658-662.
[46] M. Mecozzi, M. Pietroletti, M. Scarpiniti, R. Acquistucci, M.E. Conti, Monitoring of marine mucilage formation in Italian seas investigated by infrared spectroscopy and independent component analysis, Environmental Monitoring and Assessment 184(10) (2012) 6025-6036.
[47] V. Emmanuel, B. Odile, R. Céline, FTIR spectroscopy of woods: A new approach to study the weathering of the carving face of a sculpture, Spectrochimica Acta Part A: Molecular and Biomolecular Spectroscopy 136 (2015) 1255-1259.
[48] X. Li, Y. Wei, J. Xu, N. Xu, Y. He, Quantitative visualization of lignocellulose components in transverse sections of moso bamboo based on FTIR macro- and micro-spectroscopy coupled with chemometrics, Biotechnology for Biofuels 11(1) (2018) 263.
[49] Y. Horikawa, S. Hirano, A. Mihashi, Y. Kobayashi, S. Zhai, J. Sugiyama, Prediction of Lignin Contents from Infrared Spectroscopy: Chemical Digestion and Lignin/Biomass Ratios of Cryptomeria japonica, Applied Biochemistry and Biotechnology 188 (2019).
[50] J. Campos, J. Bao, G. Lidén, Optically pure lactic acid production from softwood-derived mannose by Pediococcus acidilactici, Journal of Biotechnology 335 (2021) 1-8.
[51] s.m. Moosavi, M. Madhoushi, M. Vakili, D. Rasouli, Evaluation of degradation in chemical compounds of wood in historical buildings using FT-IR and FT-Raman vibrational spectroscopy, Maderas. Ciencia y tecnología 21 (2019).

779 [52] A. Sharma, S. Garg, V. Sharma, ATR-FTIR spectroscopy and Machine learning for sustainable wood
780 sourcing and species Identification: Applications to wood forensics, Microchemical Journal 200
781 (2024) 110467.
782 [53] M. Seri, A. Marrocchi, The carbon–carbon triple bond as a tool to design organic semiconductors
783 for photovoltaic applications: an assessment of prospects and challenges, Journal of Materials
784 Chemistry C 9(45) (2021) 16164-16186.
785 [54] Q. Meng, J. Gao, R. Li, L. Jiang, C. Wang, H. Zhao, C. Liu, H. Li, W. Hu, New type of organic
786 semiconductors for field-effect transistors with carbon-carbon triple bonds, Journal of Materials
787 Chemistry 19(10) (2009) 1477-1482.
788 [55] X. Liu, M. Chen, Y. Wei, Assessment on oxygen enriched air co-combustion performance of
789 biomass/bituminous coal, Renewable Energy 92 (2016) 428-436.
790 [56] Y. Huang, M. Finell, S. Larsson, X. Wang, J. Zhang, R. Wei, L. Liu, Biofuel pellets made at low
791 moisture content – Influence of water in the binding mechanism of densified biomass, Biomass
792 and Bioenergy 98 (2017) 8-14.
793 [57] A. Grinberg Dana, O. Elishav, A. Bardow, G.E. Shter, G.S. Grader, Nitrogen-Based Fuels: A Power-
794 to-Fuel-to-Power Analysis, Angewandte Chemie International Edition 55(31) (2016) 8798-8805.
795 [58] O. Elishav, B. Mosevitzky Lis, E.M. Miller, D.J. Arent, A. Valera-Medina, A. Grinberg Dana, G.E. Shter,
796 G.S. Grader, Progress and Prospective of Nitrogen-Based Alternative Fuels, Chemical Reviews
797 120(12) (2020) 5352-5436.
798 [59] H. Yuan, T. Liu, Y. Liu, J. Nai, Y. Wang, W. Zhang, X. Tao, A review of biomass materials for advanced
799 lithium–sulfur batteries, Chemical Science 10(32) (2019) 7484-7495.
800 [60] P. Wang, C. Shen, B. Wang, P. Xu, L. Shen, Ammonia production from nitrogen-rich biomass
801 gasification: Nitrogen transformation from model amino acids, Fuel 326 (2022) 125071.
802 [61] W.-H. Chen, R. Aniza, A.A. Arpia, H.-J. Lo, A.T. Hoang, V. Goodarzi, J. Gao, A comparative analysis of
803 biomass torrefaction severity index prediction from machine learning, Applied Energy 324 (2022)
804 119689.
805 [62] Y. Zhang, Q. Wang, B. Li, H. Li, W. Zhao, Is there a general relationship between the exergy and
806 HHV for rice residues?, Renewable Energy 117 (2018) 37-45.
807 [63] A.C. César, J.A. Carvalho, Jr., L.F. Nascimento, Association between NOx exposure and deaths
808 caused by respiratory diseases in a medium-sized Brazilian city, Braz J Med Biol Res 48(12) (2015)
809 1130-5.
810 [64] C. Maftei, R. Muntean, I. Poinareanu, The Impact of Air Pollution on Pulmonary Diseases: A Case
811 Study from Brasov County, Romania, Atmosphere 13(6) (2022) 902.
812 [65] L.G. Fraga, J. Silva, S. Teixeira, D. Soares, M. Ferreira, J. Teixeira, Influence of Operating Conditions
813 on the Thermal Behavior and Kinetics of Pine Wood Particles Using Thermogravimetric Analysis,
814 Energies, 2020.
815 [66] J. Mularski, J. Li, A review on biomass ignition: Fundamental characteristics, measurements, and
816 predictions, Fuel 340 (2023) 127526.
817 [67] K.-T. Lee, J.-T. Du, W.-H. Chen, A.T. Ubando, K.T. Lee, Green additive to upgrade biochar from spent
818 coffee grounds by torrefaction for pollution mitigation, Environmental Pollution 285 (2021)
819 117244.
820 [68] P. Sakiewicz, K. Piotrowski, S. Kalisz, Neural network prediction of parameters of biomass ashes,
821 reused within the circular economy frame, Renewable Energy 162 (2020) 743-753.

822

Declaration of interests

☒ The authors declare that they have no known competing financial interests or personal relationships that could have appeared to influence the work reported in this paper.

☐The authors declare the following financial interests/personal relationships which may be considered as potential competing interests: